Photoinduced insulator-to-metal transition and coherent acoustic phonon propagation in $LaCoO_3$ thin films explored by femtosecond pump-probe ellipsometry

M. Zahradník,[1] M. Kiaba,[2] S. Espinoza,[1] M. Rebarz,[1] J. Andreasson,[1] O. Caha,[2] F. Abadizaman,[2] D. Munzar,[2] and A. Dubroka[2,*]

[1]*ELI Beamlines, Fyzikální ústav AV ČR, v.v.i., Za Radnicí 835, 25241 Dolní Břežany, Czech Republic*

[2]*Department of Condensed Matter Physics, Faculty of Science, Masaryk University, Kotlářská 2, 611 37 Brno, Czech Republic*

(Received 7 January 2022; revised 25 May 2022; accepted 25 May 2022; published 13 June 2022)

We have studied ultrafast dynamics of thin films of $LaCoO_3$ and $La_{0.5}Sr_{0.5}CoO_3$ with femtosecond pump-probe ellipsometry in the energy range of 1.6–3.4 eV. We have observed a large pump-induced transfer of spectral weight in $LaCoO_3$ that corresponds to an insulator-to-metal transition. The photoinduced metallic state initially relaxes via a fast process with a decay constant of about 200 fs. Both $LaCoO_3$ and $La_{0.5}Sr_{0.5}CoO_3$ exhibit a significant secondary peak in the 1–30 ps range. Results of measurements on films with different thicknesses demonstrate that it corresponds to a propagation of an acoustic strain pulse. On timescales longer than 100 ps, heat diffusion to the substrate takes place that can be modeled with a biexponential decay.

DOI: 10.1103/PhysRevB.105.235113

I. INTRODUCTION

Insulator-to-metal (IM) transitions are intriguing phenomena involving huge resistivity changes of many orders of magnitude. The transition between the insulating and the metallic ground state is typically achieved by doping, by a change in temperature, pressure, or chemical composition, or by magnetic field [1]. In $LaCoO_3$, an IM transition can be induced both by doping and by changing the temperature. With hole doping, usually achieved with the exchange of trivalent La^{3+} with a divalent ion, e.g., Sr in the $La_{1-x}Sr_xCoO_3$ compound, a ferromagnetic metallic state is developed for $x > 0.18$ [2,3]. $LaCoO_3$ is a diamagnetic insulator below 50 K; however, in the intermediate-temperature range between 100 and 400 K, it exhibits semiconducting and paramagnetic behavior, and above about 500 K it turns into a bad metal [4]. The physics of the cobaltites is considerably complicated by a quasidegeneracy between the low-spin (LS; $t_{2g}^6 e_g^0$), intermediate-spin (IS; $t_{2g}^5 e_g^1$) and high-spin (HS; $t_{2g}^4 e_g^2$) states of a Co ion. This is due to the competition between the Hund's rule coupling and the crystal field splitting [5]. The question of which spin state dominates in the cobaltites has been a subject of intense debate lasting over many decades [6–16].

Femtosecond pump-probe spectroscopies [17] have been used to study the pump-induced IM transitions in many materials, e.g., in cuprates [18], vanadates [19], nickelates [20,21], and organics [22]. Concerning cobaltites, Okimoto *et al.* [23] found transient features on picosecond timescales in $Pr_{0.5}Ca_{0.5}CoO_3$ that were interpreted, based on model calculations, to be a consequence of the propagation of a photonically created metallic domain at the velocity of the ultrasonic wave. Izquierdo *et al.* [24] examined $LaCoO_3$ using femtosecond soft x-ray spectroscopy and found picosecond transient features that were interpreted in terms of a model involving several steps of the bulk pump-induced metallization process. Opinions on which transient features are due to bulk processes and which are due to the propagation of a domain or wave remain contradictory. We reexamine the pump-induced optical response of cobaltites with femtosecond ellipsometry that was recently developed [25–28]. Ellipsometry is a self-normalizing technique that allows one to determine very accurately and reproducibly the complex dielectric function without a need for Kramers-Kronig analysis. Here we report on the pump-probe ellipsometric study of $La_{1-x}Sr_xCoO_3$ thin films with $x = 0$ and $x = 0.5$. In the $x = 0$ compound, we have observed a large pump-induced redistribution of the optical spectral weight from high to low energies that is indicative of the IM transition. In order to discern which transient features correspond to bulk phenomena and which correspond to the propagation of a wave, we investigated several thin films with different thicknesses. The data show that the dynamics on the picosecond timescale probed using visible wavelengths is a consequence of strain pulse (the so-called coherent acoustic phonon) propagation [29] possibly accompanied by an increased concentration of excited spin states (IS and/or HS).

II. EXPERIMENT

Several films of $LaCoO_3$ and $La_{0.5}Sr_{0.5}CoO_3$ were grown by pulsed laser deposition on 10 × 10 mm^2 substrates of $(La_{0.7}Sr_{0.3}) \times (Al_{0.65}Ta_{0.35})O_3$ (LSAT) at 700 °C and 0.1 mbar oxygen partial pressure using a fluency of 2 J/cm^2 for the excimer laser with a wavelength of 248 nm. The samples were postannealed at 550 °C for 3 h in a room pressure oxygen atmosphere to decrease oxygen-vacancy concentration. X-ray diffraction measurements confirmed that the films are epitaxial and films with thickness below 100 nm are fully strained. Such films grown on an LSAT substrate can exhibit strain-induced ferromagnetism below 90 K [30]. Our measurements were, however, performed at room temperature,

*dubroka@physics.muni.cz

far above the possible ferromagnetic phase. The thickness of the films d was determined using x-ray reflectometry and ellipsometry.

Time-resolved spectroscopic ellipsometry measurements were performed using a femtosecond pump-probe ellipsometer at ELI Beamlines [25]. The system was based on an amplified Ti:sapphire laser (Coherent Astrella) with its fundamental mode of 35 fs pulses at 800 nm with a 1 kHz repetition rate and pulse energy of 6 mJ. About 10 μJ of the fundamental beam was employed as a pump beam and was focused on a sample so that the fluency was about 3 mJ/cm^2. About 1 μJ was used to generate supercontinuum white light in a CaF_2 window, which served as a probe beam, allowing us to investigate the spectral range from about 1.6 to about 3.4 eV. The time resolution of the setup is ultimately limited by the temporal cross correlation of the pump and probe pulses, and it was experimentally determined to be 100 fs. The maximal pump-probe delay is about 6 ns due to the limited length of the optical delay line. The measurements were carried out at angle of incidence $\alpha = 60°$, and the angle of incidence of the pump beam was 55°. In the polarizer-sample-compensator-analyzer configuration with a rotating compensator, transient reflectance-difference spectra were measured by scanning the pump-probe delay. The data were acquired repeatedly for multiple different azimuth angles of the compensator while the polarizer and analyzer were kept fixed at ±45°. In order to calculate the ellipsometric angles from the series of measurements at different compensator angles, the Müller matrix formalism was employed for each photon energy and delay time, where the obtained reflectance-difference spectra were processed by Moore-Penrose pseudoinversion using reference equilibrium-state spectra. Further details on the experimental setup, as well as the data evaluation procedure, can be found elsewhere [26–28]. The equilibrium-state ellipsometric data were measured using a Woollam VASE ellipsometer in the 0.6–6.5 eV range and a Woollam IR-VASE ellipsometer in the 0.05–0.6 eV range.

All ellipsometric data were analyzed using the standard model of coherent interferences in a thin film on a substrate [31]. The optical response of the substrate was measured on a bare substrate. The substrate did not exhibit any significant pump-induced response. The dielectric function employed in the analysis of the pump-probe ellipsometry data of thin films was modeled as a sum of the Lorentz oscillators [31]. The equilibrium ellipsometric data were analyzed at each photon energy (the so-called point-by-point fit). Following this procedure, the obtained equilibrium spectra represent the optical response of a thin film that is, in principle, independent of the film thickness. In the case of the pump-probe ellipsometry, some aspects of the data similarly reflect the change in the optical constants of the material and should be independent of the film thickness for thicknesses sufficiently smaller than the pump penetration depth. However, additionally, the data may involve features corresponding, e.g., to propagation of a strain pulse [29,32] and to thermal diffusion [17], which are, in principle, thickness dependent. Consequently, the obtained optical spectra represent pseudo-optical constants reflecting the overall response of the heterostructure. One possibility of how to discern one type of phenomenon from the other is by examining films with

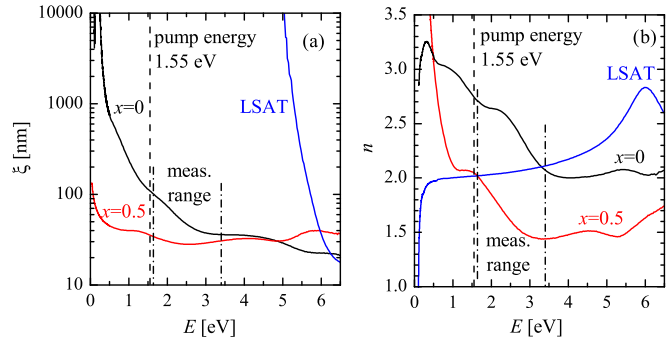

FIG. 1. (a) Penetration depth and (b) the index of refraction of $La_{1-x}Sr_xCoO_3$ thin films with $x = 0$ (black solid line), $x = 0.5$ (red solid line), and LSAT substrate (blue solid line). The dashed and dash-dotted lines denote the pump energy and limits of the measurement range, respectively.

various thicknesses as we do in the present work. Figures 1(a) and 1(b) display the penetration depth ξ and the real part of the index of refraction n, respectively, of $La_{1-x}Sr_xCoO_3$ thin films with $x = 0$ and $x = 0.5$ obtained using the equilibrium ellipsometry. Penetration depth was determined from the imaginary part of the index of refraction k as $\xi = \lambda/(2\pi k)$, where λ is the vacuum wavelength of the radiation. The penetration depth at an energy of the pump of 1.55 eV (dashed vertical line) is about 110 and 35 nm for $x = 0$ and $x = 0.5$, respectively.

In the rest of the paper, we display the obtained (pseudo-)optical constants in terms of the real part of the optical conductivity σ_1 related to the imaginary part of the dielectric function ε_2 as $\sigma_1(\omega) = \varepsilon_0\omega\varepsilon_2(\omega)$. The quantity σ_1 is used to describe the absorption of radiation, and it obeys the conductivity sum rule [33]. The information represented by σ_1 is complemented by that contained in the real part of the dielectric function ε_1, representing the so-called inductive response.

III. DATA ANALYSIS AND DISCUSSION

Section III A is devoted to spectral analysis of the maximum pump-induced response which occurs near 200 fs. In Sec. III B, we analyze the transient response in the whole range of delays, i.e., from 50 fs to 5 ns.

A. Maximum pump-induced response near 200 fs

Figure 2(a) displays the real part of the optical conductivity σ_1, and Fig. 2(b) shows the real part of the dielectric function ε_1 of the equilibrium response of $x = 0$ ($d = 100$ nm) and $x = 0.5$ ($d = 31$ nm) thin films obtained by conventional ellipsometry (black solid lines). The pump-probe data for the two compounds before the pump (0 fs delay) are also displayed (green thick solid lines), and they essentially overlap with the equilibrium data. Similar to previous reports [4,34], the equilibrium spectrum of σ_1 of the parent compound ($x = 0$) exhibits a small band gap of about 0.2 eV and several interband transitions. According to Ref. [34], there are $t_{2g} \rightarrow t_{2g}$ transitions near 0.4 eV, $t_{2g} \rightarrow e_g$ transitions near 1.5 eV, and O $2p \rightarrow$ Co e_g transitions near 3 eV. The 1.5 eV pump thus falls

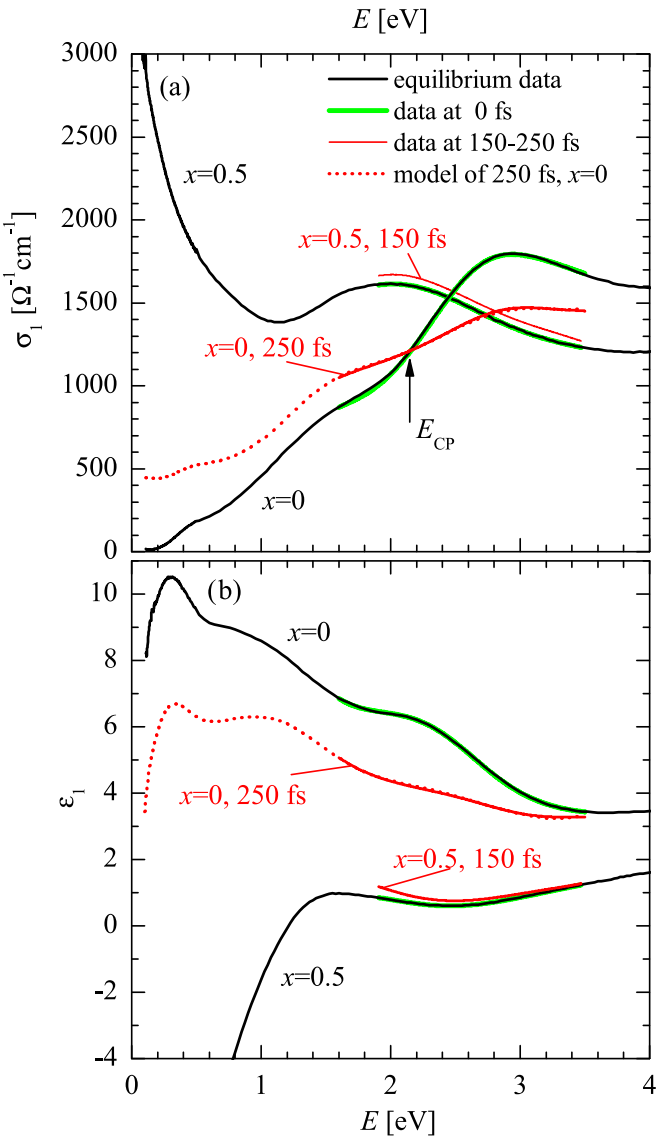

FIG. 2. (a) Real part of the optical conductivity σ_1 and (b) the real part of the dielectric function ε_1 at room temperature of $La_{1-x}Sr_xCoO_3$ films with $x = 0$ and a thickness of 100 nm and $x = 0.5$ and a thickness of 31 nm. Panels show the equilibrium data (black lines) and the pump-probe data before the pump, i.e., at 0 fs delay (green thick solid lines) and at delays corresponding to the largest pump-induced response of 250 fs ($x = 0$) and 150 fs ($x = 0.5$) (solid red lines). The red dotted lines represent Kramers-Kronig consistent extrapolations of the $x = 0$ spectra at 250 fs to lower energies as detailed in the text. The arrow in (a) denotes the crossing point at $E = E_{CP}$.

in the energy range of $t_{2g} \rightarrow e_g$ transitions. The conductivity spectrum of the doped sample ($x = 0.5$) displays features similar to those of $x = 0.3$ [35]; that is, at low energies it exhibits a Drude peak describing the metallic response, and at higher energies it exhibits interband transitions with a band near 2 eV. The spectrum of $\varepsilon_1(x = 0)$ [see Fig. 2(b)] exhibits, below 1 eV, positive values in the range from 8 to 10 that are characteristic of an insulator, and the spectrum of $\varepsilon_1(x = 0.5)$ exhibits, below 1.5 eV, a decrease to negative values with decreasing energy, which is typical for a metallic response.

Figures 2(a) and 2(b) also display spectra at delays corresponding to the maximum pump-probe response, i.e., at a 250 fs delay for the $x = 0$ sample and at a 150 fs delay for the $x = 0.5$ sample (red solid lines). The spectrum of $\sigma_1(x = 0, 250\text{ fs})$ exhibits a significant suppression of the band at 3 eV and an increase of the conductivity below the crossing point at $E_{CP} = 2.1$ eV. Clearly, the pump causes a shift in optical spectral weight from energies above E_{CP} towards energies below. Recall that the optical spectral weight per a frequency interval (ω_1, ω_2) is defined as $\int_{\omega_1}^{\omega_2} \sigma_1(\omega) d\omega$. The spectrum of $\varepsilon_1(x = 0, 250\text{ fs})$ is markedly decreased with respect to the equilibrium one [see Fig. 2(b)], which, as we show below, also reflects the pump-induced shift of the spectral weight to lower energies.

Further insight into the pump-induced response of the $x = 0$ sample can be obtained by analyzing of the data with a Kramers-Kronig consistent model. We have modeled the equilibrium dielectric function as a sum of several Kramers-Kronig consistent contributions, $\varepsilon(\omega) = \sum_j \varepsilon_{G,j}(\omega) + \sum_j \varepsilon_{T-L,j}(\omega)$, where $\varepsilon_G(\omega)$ stands for a Gaussian and $\varepsilon_{T-L}(\omega)$ stands for a Tauc-Lorentz term [31]. The fit of the model to the equilibrium data provides spectra of σ_1 and ε_1 essentially overlapping with those in Fig. 2 (fit not shown). For the 250 fs data, the model dielectric function was complemented by the Drude term, $\varepsilon_D(\omega) = -\omega_{pl}^2/\omega(\omega + i\gamma_D)$, where ω_{pl} is the plasma frequency and γ_D is the broadening parameter. We have fitted the model function to the data at 250 fs with only a limited number of free parameters (in particular, ω_{pl}, the parameters of the 3 eV band and of a band at higher energies) so that the overall shape of the response is conserved. The resulting model spectra [displayed as red dotted lines in Figs. 2(a) and 2(b)] reveal that the conductivity and thus the spectral weight increase even below the lowest energy of our measurements of 1.6 eV. The fits are not sensitive to details of the low-energy conductivity, such as the broadening of the Drude term γ_D, which was fixed at 1 eV. Nevertheless, it is reasonably sensitive to the increase of the low-energy spectral weight, which is essentially given by ω_{pl}^2, for which the fitting yielded $\omega_{pl}^2 = (3.3 \pm 0.1)\ \text{eV}^2$. This sensitivity comes predominantly from the pump-induced decrease of $\varepsilon_1(x = 0)$ [see Fig. 2(b)], which is a typical signature of the formation of a metallic (Drude) contribution. The corresponding number of charge carriers per cobalt ion can be calculated from ω_{pl}^2 using the standard Drude formula $N = \epsilon_0 m^* \omega_{pl}^2 a^3/e^2$, where m^* stands for the effective mass and $a = 3.8$ Å is the lattice parameter. Provided m^* equals the free-electron mass, we obtain $N \approx 0.13$, which is a sizable amount of charge per Co ion, comparable, e.g., to the one generated by photodoping charge carriers in a halogen-bridged nickel-chain compound [21].

Regardless of the uncertainties about the details of the pump-induced spectrum of σ_1 below 1.6 eV (which call for exploration in future), our analysis clearly shows the main trend: the pump induces a large transfer of spectral weight from energies above E_{CP} to lower energies; that is, the material very likely becomes metallic. This trend can also be deduced simply from the measured pump-induced spectra in Fig. 2 [both $\sigma_1(x = 0)$ and $\varepsilon_1(x = 0)$]. They shift to some extent towards the spectra of the metallic $x = 0.5$ sample. Such a transfer of spectral weight can be expected because $LaCoO_3$ exhibits a

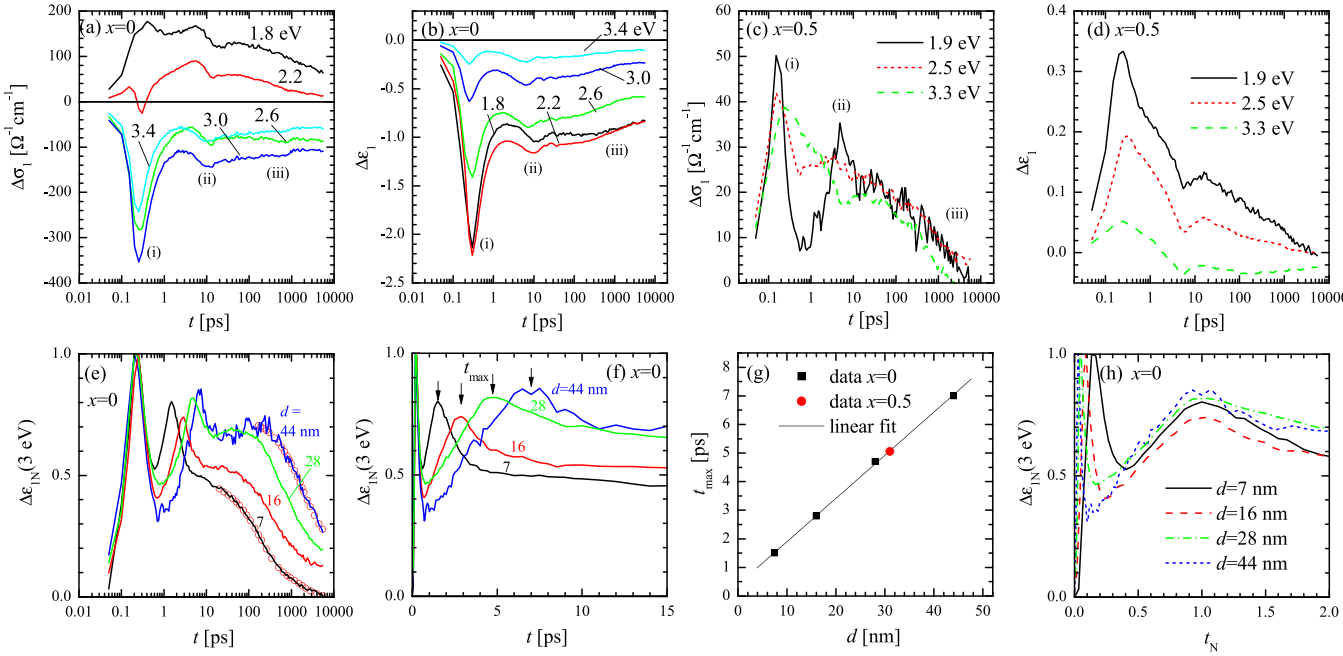

FIG. 3. Transient signals relative to the values before the pump (a) and (c) of the real part of the conductivity $\Delta\sigma_1$ and (b) and (d) of the real part of the dielectric function $\Delta\varepsilon_1$ of $La_{1-x}Sr_xCoO_3$ films with (a) and (b) $x = 0$ and a thickness 100 nm and (c) and (d) $x = 0.5$ and a thickness of 31 nm at selected probe photon energies as shown in the graphs. (e) and (f) $\Delta\varepsilon_1$ transients at 3 eV normalized to the maximum values near 250 fs $\Delta\varepsilon_{1N}(3\text{ eV})$ for several $x = 0$ films with thicknesses d specified in the panels. Red circles in (e) represent fits by the biexponential decay model detailed in the text. (g) The delays of the maxima t_{max}, denoted by arrows in (f), versus the film thickness d. (h) Transients from (f) as a function of the normalized delay $t_N = t/t_{max}$. All data were measured at room temperature.

thermally induced IM transition which is, in the equilibrium optical response, indeed accompanied by a transfer of spectral weight from high energies (above 1.4 eV) to lower energies, giving rise to a Drude peak [4]. In order to roughly estimate the pump-induced electronic temperature, we can compare our results with the equilibrium spectra obtained at high temperatures [4]. The extrapolated DC conductivity at 250 fs of about 500 $\Omega^{-1}\,\text{cm}^{-1}$ corresponds to a temperature of the equilibrium spectra in the range between 500 and 600 K [4].

Concerning the $x = 0.5$ sample, both σ_1(150 fs) and ε_1(150 fs) are slightly higher than the equilibrium spectra [see Figs. 2(a) and 2(b)]. A similar trend with increasing temperature in this energy range has been observed on metallic $La_{1-x}Sr_xCoO_3$ with $x = 0.3$ (see Ref. [35]). Such changes at energies higher than the Drude isosbestic point of 0.3 eV [35] reflect an increase of the Drude scattering rate γ_D. The latter is expected for a metallic sample if charge carriers get comparably more disturbed by excited quasiparticles. In other words, in the $x = 0.5$ sample, the direction of the pump-induced spectral weight transfer is upward in energy and thus opposite to that of the $x = 0$ sample.

B. Analysis of the transients at time delays between 50 fs and 5 ns

Figures 3(a) and 3(b) display the transient optical constants at delay t relative to the values before the pump, $\Delta\sigma_1 = \sigma_1(t) - \sigma_1(t = 0)$ and $\Delta\varepsilon_1 = \varepsilon_1(t) - \varepsilon_1(t = 0)$, respectively, at selected energies for the $x = 0$ film with $d = 100$ nm. The transient signals exhibit the following general trend: (i) First, they reach a peak value near 250 fs. This is followed by a fast relaxation with a characteristic decay time of about 200 fs. (ii) Another transient structure emerges between 1 and 30 ps, forming a secondary maximum. (iii) For times longer than 100 ps the signals monotonically decrease within the measurement delay span of 5000 ps. Note that the transients with the largest overall values $\Delta\sigma_1$ at probe photon energy 3 eV, $\Delta\sigma_1$(3 eV), and $\Delta\varepsilon_1$ at probe photon energy 2.2 eV, $\Delta\varepsilon_1$(2.2 eV), have very similar profiles. This can be understood since, by virtue of the Kramers-Kronig relations, $\Delta\varepsilon_1$ at a given energy E is a certain measure of the spectral weight transferred across E. Therefore, $\Delta\varepsilon_1$(2.2 eV) near $E_{CP} \approx 2.1$ eV follows the decrease of the 3 eV band [tracked by $\Delta\sigma_1$(3 eV)], whose spectral weight is partially transferred, after the pump, to energies lower than E_{CP}.

Figures 3(c) and 3(d) display the transient difference optical constants, $\Delta\sigma_1$ and $\Delta\varepsilon_1$, respectively, at selected energies for the $x = 0.5$ film with $d = 31$ nm. The $\Delta\sigma_1$(1.9 eV) transient [see Fig. 3(c)] exhibits (i) a peak near 150 fs that relaxes with a decay time of about 100 fs and also (ii) a pronounced secondary peak between 1 and 10 ps. Notably, these features are similar to features (i) and (ii) of the thin film with $x = 0$. The signs of both transients, however, here are positive, and the maximum values are almost an order of magnitude smaller than in the case of $x = 0$.

The pump-probe response of a 100 nm $LaCoO_3$ thin film was studied by Bielecki *et al.* using femtosecond reflectometry at 3.2 eV [36]. Their data are very similar to our $\Delta\varepsilon_1$ transients at 3.0 or 3.4 eV. They also observed the secondary peak, and it was interpreted along the lines of a previous study by Okimoto *et al.* [23]. The authors of the latter study reported a similar

feature at picosecond timescale in the data for polycrystalline $Pr_{0.5}Ca_{0.5}CoO_3$ and concluded, on the basis of the results of model computations, that the structure is due to a propagation of a metallic domain at a velocity of 4.4 km/s. This conclusion inspired us to test this hypothesis more directly by measuring the transient response on $x = 0$ films with various thicknesses between 7 and 44 nm. Obtained $\Delta\varepsilon_1$(3 eV) transients normalized to the value at the first peak near 250 fs, denoted $\Delta\varepsilon_{1N}$(3 eV), are shown in Figs. 3(e) and 3(f) on logarithmic and decadic scales, respectively. The data clearly show that the delay of the secondary peak t_{max} [marked by the arrows in Fig. 3(f)] increases with increasing film thickness. This is indeed a typical signature of the propagation of an acoustic strain pulse between the surface and the film-substrate interface (see, e.g., Refs. [29,32,37]). Figure 3(g) demonstrates that t_{max} is a linear function of d. Similar to the authors of Ref. [32], we assume that t_{max} corresponds to the time of propagation of the pulse with velocity v between the surface and the interface, i.e., $t_{max} = d/v$. Consequently, we obtain for each sample the corresponding velocity and the average velocity of all samples of $v = (5.7 \pm 0.5)$ nm/ps. Notably, the value of the $x = 0.5$ film, obtained from the transient $\Delta\sigma_1$(1.9 eV) [see Fig. 3(c)], represented in Fig. 3(g) by the red circle, fits very well to the linear dependence, demonstrating that the optical signatures of the propagation of the strain pulse are universal in cobaltites, independent of whether the electronic ground state is metallic or insulating.

Interestingly, the width of the secondary peak in Fig. 3(f) also scales with the film thickness. Figure 3(h) displays these data as a function of the delay normalized to that of the secondary maximum, $t_N = t/t_{max}$. All the transients display a triangular shape in which the signal increases linearly until it reaches the maximum at $t_N = 1$ and then it gradually decreases. We propose the following picture for the formation of the transient profile displayed in Fig. 3(h): First, the strain pulse is formed by the pump at the surface, which we assume as in Ref. [29], and it propagates towards the interface. Note that the contribution of the pulse to the strain profile (see the theoretical prediction displayed in Fig. 3 of Ref. [29]) is essentially antisymmetric with respect to the pulse front; that is, it exhibits negative strain before the front and positive strain after the front. Consequently, as the strain pulse propagates from the film surface to the interface, the average value of the strain in the whole film gradually increases. Second, the strain modulation generates a pronounced change in electronic and optical properties. Recall that cobaltites are very susceptible to strain [30]; for example, with an increasing hydrostatic component of the strain tensor, the crystal field splitting decreases (see Refs. [38,39]), which may cause an increase of the population of IS and/or HS sites. Third, as the pulse propagates for $t_N < 1$, the effective optical constant $\Delta\varepsilon_{1N}$, given in the present case with $d < \lambda/(4n)$ essentially by the average value of the optical constant in the whole film, gradually increases and culminates when the pulse reaches the interface at $t_N = 1$. Afterward, the pulse propagates to the substrate, where it does not give rise to a significant transient signal. The film gradually relaxes, and $\Delta\varepsilon_{1N}$ decreases for $t_N > 1$.

Here we discuss the sign of the secondary peak in $\Delta\sigma_1$ and $\Delta\varepsilon_1$ compared to the first peak. We speculate that the strain modulation causes an increase of the population of excited spin states (IS and/or HS) in the region of positive strain left behind the pulse front. Since the increase of the population of the excited spin states in $LaCoO_3$ with increasing temperature [16] is accompanied by a shift of spectral weight from high to low energies [4], we would expect a similar effect in our measurements. Indeed, we observe that the secondary peak has the same sign in both $\Delta\sigma_1$ [see Fig. 3(a)] and $\Delta\varepsilon_1$ [see Fig. 3(b)] as the first peak, which corresponds to a shift of spectral weight to low energies, as we showed in Sec. III A. Note that the changes in the electronic configuration occur on timescales shorter than the relaxation time of 0.2 ps of the first transient peak. Consequently, they are fast enough to follow the picosecond dynamics of the strain-pulse propagation. In the case of the metallic $x = 0.5$ sample, provided that the same physical picture applies, the increased concentration of excited spin states may enhance the scattering of charge carriers and thus broaden the Drude peak, as we observe in Fig. 3(c).

A strain pulse can be formed also at the interface and propagate towards the surface, as considered, e.g., in Ref. [32]. Although we do not exclude that such a contribution occurs in the data, we believe that this process is less important since the optical contrast at the interface is smaller than the one at the surface [see Fig. 1(b)]. Even in this case the equation $t_{max} = d/v$ would be valid. The transient response might, in addition, display structures due to acoustic echoes of the strain pulse reflected from the interface that occur at $t = 2d/v$ [29]. Based on our independent estimate of the velocity presented below, however, we can exclude the possibility that the structure centered at $t_N = 1$ in Fig. 3(h) is due to such an echo.

The velocity of a strain pulse can also be determined from the period of oscillations of the transient signal (so-called Brillouin oscillations) in a film with large thickness (or in a bulk) [29,32,40]. These oscillations arise due to interference involving the probe beam reflected from the front of the strain pulse. The profile has been predicted to be an oscillatory function with period [41]

$$\tau = \frac{1}{2v}\frac{\lambda}{n\cos\beta}, \tag{1}$$

where n is the real part of the index of refraction and β is the angle of refraction inside the film determined from Snell's law as $\cos\beta = \sqrt{1 - \sin^2(\alpha)/n^2}$. Equation (1) was obtained using the expression for the phase factor occurring in the description of interference in a thin film [31]. In addition, the oscillatory profile is exponentially damped on the timescale given by ξ/v. Based on the above-obtained velocity v, the expected τ for $LaCoO_3$ at a probe energy of 3 eV ($n = 2.2$) amounts to 18 ps. The samples in Fig. 3(e) have small thicknesses so that the strain pulse reaches the interface before it gives rise to the oscillatory behavior. In order to explore the oscillatory transients in $LaCoO_3$, we have investigated a thicker film with $d = 188$ nm. For such a relatively large thickness, the strain pulse reaches the interface at delays larger than 30 ps. Figure 4(a) displays the obtained normalized $\Delta\varepsilon_1$ transients at selected energies. The transients display the main secondary peak between 6 and 12 ps whose delay decreases with increasing probe energy (see the dashed line). The maximum

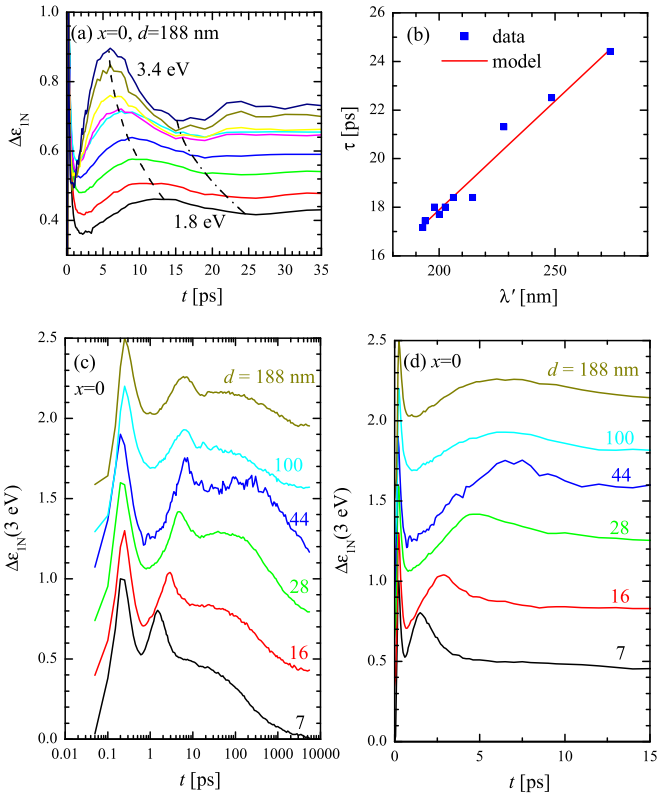

FIG. 4. (a) Normalized $\Delta\varepsilon_{1N}$ transients of a $LaCoO_3$ film with a thickness of 188 nm at selected energies between 1.8 and 3.4 eV (with 0.2 eV steps). The dashed and dash-dotted lines are guides to the eye. (b) Period τ as a function of $\lambda' = \lambda/(n\cos\beta)$. The line corresponds to Eq. (1) with $v = 5.6$ nm/ps. (c) and (d) An overview of the normalized $\Delta\varepsilon_{1N}(3\text{ eV})$ transients of all samples on semilogarithmic and linear scales, respectively. For clarity, the transients are shifted vertically.

is followed by a shallow minimum (see the dash-dotted line). The oscillatory behavior is quickly damped because of the small penetration depth ξ [see Fig. 1(a)]. From the delays of this maximum and of the minimum, we can calculate the period of the oscillations τ and, using Eq. (1), the velocity v. The obtained average value of the velocity amounts to $v = (5.6 \pm 0.2)$ nm/ps, which agrees very well with the value found above and with the value of 5.9 nm/ps reported in Ref. [36]. The experimental values of τ (squares) are plotted in Fig. 4(b) as a function of $\lambda' = \lambda/(n\cos\beta)$ together with the dependence given by Eq. (1) with $v = 5.6$ nm/ps. It can be seen that the relation (1) tracks the data very well. The transients displayed in Fig. 4(a) exhibit the trend observed earlier on picosecond timescales in $Pr_{0.5}Ca_{0.5}CoO_3$ [23]: The maximum shifts to shorter delays with increasing energy of the probe. Our data show that the secondary peak is not limited to the case of the first-order insulator-metal transition of the latter compound and is common to cobaltites, including our metallic $x = 0.5$ sample, and as we showed above, it corresponds to the propagation of a strain pulse possibly accompanied by an increased concentration of excited spin states.

For the sake of an overview and comparison, Figs. 4(c) and 4(d) display $\Delta\varepsilon_{1N}(3\text{ eV})$ data for all our $x = 0$ samples on semilogarithmic and linear scales, respectively. Note the difference between the shape of the secondary peak in thin films ($d = 7$–44 nm) and that in thick films ($d = 100$ and 188 nm). In the former, the secondary maximum occurs at a delay that increases with d, and the shape is close to a triangle. In thicker films, the secondary maximum occurs at a delay which is not increasing with d, and its profile is rounded. This difference corresponds to the different origins of the structures as discussed above.

Next, we address in more detail the metallization near 200 fs and the following fast relaxation. Figure 3(e) demonstrates that, unlike the processes for delays longer than 1 ps, this feature is essentially independent of the film thickness and thus reflects a bulk phenomenon occurring essentially homogeneously within the film. Note that the thicknesses of the films in Fig. 3(e) are smaller than the pump penetration depth of about 110 nm. This fast relaxation can be modeled with an exponential decay (not shown), with a decay constant of about 200 fs. This is a typical relaxation time of excited electrons losing their energy by emitting phonons [17]. Near 1 ps, this fast relaxation is essentially over, and the amount of spectral weight transferred across E_{CP} back to higher energies, as represented by $\Delta\varepsilon_1(2.2\text{ eV})$, in the 100 nm thick film equals approximately 50% of the maximum value [see Fig. 3(b)]. It is likely that at this delay, electron and phonon degrees of freedom of the film are essentially in thermal equilibrium [17]. The consecutive evolution of $\Delta\varepsilon_1(2.2\text{ eV})$, similar to that of $\Delta\sigma_1(3\text{ eV})$, is only weakly modulated by the pulse propagation—the variations of the signal connected to the secondary peak are, in these transients, about 10 times weaker than the first peak. Note that at higher energies, the relative magnitude of the secondary peak in comparison to the first peak increases; see the $\Delta\varepsilon_1(3\text{ eV})$ and $\Delta\varepsilon_1(3.4\text{ eV})$ data in Fig. 3(b): In $\Delta\varepsilon_1(3\text{ eV})$, the relative magnitude of the secondary peak is considerably larger than in $\Delta\varepsilon_1(2.2\text{ eV})$, and in $\Delta\varepsilon_1(3.4\text{ eV})$, the two peaks have roughly the same magnitude. This trend is probably related to the fact that the strain pulse induces transfers of spectral weight from energies higher than those involved in the formation of the first transient peak. Above about 100 ps, the film starts to cool down significantly as the heat diffuses to the substrate.

The fast relaxation in a $LaCoO_3$ thin film was also examined by Bielecki *et al.* [36]. As in the present work, they found a fast decay on the 100 fs timescale and, in addition, its significant temperature dependence. Their analysis showed that the data follow the Fermi statistics with a spin gap of 17 meV that seems to correspond to the HS-LS splitting [16]. In a recent femtosecond soft x-ray spectroscopy study of bulk $LaCoO_3$, a fast relaxation with 170 fs decay time and a pronounced secondary maximum near 1.5 ps were reported [24]. These features were interpreted as bulk phenomena due to several steps in the metallization process. The fast relaxation with the decay constant of 170 fs compares very well to the profile of our first peak, labeled (i) in Fig. 3. Concerning the maximum near 1.5 ps, the transients of our thickest films do not seem to exhibit any sharp structure near this delay [see Figs. 4(a) and 3(b)]. Our data for delays larger than 1 ps, however, depend on the probe wavelength; therefore, it is not possible to compare them in a simple way with the data at soft x-ray wavelengths. Concerning the $x = 0.5$ sample, the

fast relaxation of the first transient peak of $\Delta\sigma_1(1.9\ \text{eV})$ [see Fig. 3(c)] can be modeled by an exponential decay with a time constant of 90 fs; this estimate may be limited by the time resolution of the setup.

The process labeled (iii) in Fig. 3 on timescales larger than 100 ps presumably corresponds to heat diffusion [17] to the substrate which is transparent for the pump beam. The transients shown in Fig. 3(e) demonstrate that the cooling process is slower for thicker films. The reason is that with increasing film thickness, the total energy absorbed per surface area increases and the heat has a longer diffusion path before it reaches the substrate. In this delay range the transients can be well modeled by a biexponential decay, $A\exp(-t/t_A) + B\exp(-t/t_B)$. This is documented by the fit of the transient of the $d = 7$ nm sample, represented by the red circles in Fig. 3(e), with relaxation times $t_A = 180$ ps and $t_B = 1700$ ps. For the thicker sample with $d = 44$ nm, a two-step decay is also visible, but only the first component with $t_A = 1800$ ps can be fitted with reliable accuracy, whereas the relaxation time t_B cannot be reliably determined by the present setup (see Sec. II) and can be assumed to be longer than 6 ns. For even thicker films with $d = 100$ and 188 nm, the cooling process takes much longer and cannot be measured by our setup. A biexponential heat diffusion was also found in manganite films [42].

IV. SUMMARY

The main findings of our investigations of the pump-probe optical response of $LaCoO_3$ thin films can be summarized as follows: (i) Within the first 200 fs after the pump, a transfer of optical spectral weight occurs, from high energies above 2.1 eV to lower energies, and we interpret it to be a consequence of the insulator-to-metal transition. The magnitude of the effect corresponds to about 0.13 electron per Co ion. Within the next about 200 ps, this photoinduced metallic state relaxes back, whereby the conductivity differences decrease to about 50% of the maximum values. These features are essentially independent of film thickness, and thus, they correspond to a bulk excitation/relaxation within the penetration depth of the pump. (ii) Between 1 and 30 ps additional features appear that are due to the propagation of an acoustic strain pulse at a velocity of 5.6 ± 0.2 nm/ps. We observe similar phenomena also in the metallic $La_{0.5}Sr_{0.5}CoO_3$. We speculate that the strain pulse is accompanied by an increased concentration of excited spin states (intermediate and/or high spin). (iii) For delay times longer than 100 ps, we observe a heat film-to-substrate diffusion that can be modeled with a biexponential decay.

ACKNOWLEDGMENTS

We acknowledge fruitful discussions with J. Bielecki, F. F. Delatowski, D. Geffroy, and J. Kuneš. We thank M. Golian for supporting measurements. This work was financially supported by the MEYS of the Czech Republic under the project CEITEC 2020 (LQ1601), by the Czech Science Foundation (GAČR) under Project No. GA20-10377S, and by the Operational Programme Research, Development and Education Project "Postdoc2MUNI" (Grant No. CZ.02.2.69/0.0/0.0/18_053/0016952). CzechNanoLab Project No. LM2018110 funded by MEYS CR is gratefully acknowledged for the financial support of the measurements and sample fabrication at CEITEC Nano Research Infrastructure. M.Z., S.E., M.R., and J.A. acknowledge the support of the ELIBIO (Grant No. CZ.02.1.01/0.0/0.0/15-003/0000447) and ADONIS (Grant No. CZ.02.1.01/0.0/0.0/16-019/0000789) projects from the European Regional Development Fund. We acknowledge LM2017094, MEYS–Large research infrastructure project ELI Beamlines in Dolní Břežany, Czech Republic, for provision of laser beam time and would like to thank the instrument group and facility staff for their assistance.

[1] M. Imada, A. Fujimori, and Y. Tokura, Rev. Mod. Phys. **70**, 1039 (1998).
[2] J. Wu and C. Leighton, Phys. Rev. B **67**, 174408 (2003).
[3] D. Samal and P. S. A. Kumar, J. Phys.: Condens. Matter **23**, 016001 (2011).
[4] Y. Tokura, Y. Okimoto, S. Yamaguchi, H. Taniguchi, T. Kimura, and H. Takagi, Phys. Rev. B **58**, R1699 (1998).
[5] S. Maekawa, T. Tohyama, S. E. Barnes, S. Ishihara, W. Koshibae, and G. Khaliullin, *Physics of Transition Metal Oxides* (Springer, Berlin, 2004).
[6] F. M. F. de Groot, J. C. Fuggle, B. T. Thole, and G. A. Sawatzky, Phys. Rev. B **42**, 5459 (1990).
[7] M. A. Korotin, S. Y. Ezhov, I. V. Solovyev, V. I. Anisimov, D. I. Khomskii, and G. A. Sawatzky, Phys. Rev. B **54**, 5309 (1996).
[8] C. Zobel, M. Kriener, D. Bruns, J. Baier, M. Gruninger, T. Lorenz, P. Reutler, and A. Revcolevschi, Phys. Rev. B **66**, 020402(R) (2002).
[9] A. Ishikawa, J. Nohara, and S. Sugai, Phys. Rev. Lett. **93**, 136401 (2004).
[10] J. Q. Yan, J. S. Zhou, and J. B. Goodenough, Phys. Rev. B **69**, 134409 (2004).
[11] M. W. Haverkort, Z. Hu, J. C. Cezar, T. Burnus, H. Hartmann, M. Reuther, C. Zobel, T. Lorenz, A. Tanaka, N. B. Brookes, H. H. Hsieh, H. J. Lin, C. T. Chen, and L. H. Tjeng, Phys. Rev. Lett. **97**, 176405 (2006).
[12] Z. Ropka and R. J. Radwanski, Phys. Rev. B **67**, 172401 (2003).
[13] A. Podlesnyak, S. Streule, J. Mesot, M. Medarde, E. Pomjakushina, K. Conder, A. Tanaka, M. W. Haverkort, and D. I. Khomskii, Phys. Rev. Lett. **97**, 247208 (2006).
[14] M. Merz, P. Nagel, C. Pinta, A. Samartsev, H. v. Löhneysen, M. Wissinger, S. Uebe, A. Assmann, D. Fuchs, and S. Schuppler, Phys. Rev. B **82**, 174416 (2010).
[15] V. Křápek, P. Novák, J. Kuneš, D. Novoselov, D. M. Korotin, and V. I. Anisimov, Phys. Rev. B **86**, 195104 (2012).
[16] A. Hariki, R.-P. Wang, A. Sotnikov, K. Tomiyasu, D. Betto, N. B. Brookes, Y. Uemura, M. Ghiasi, F. M. F. de Groot, and J. Kuneš, Phys. Rev. B **101**, 245162 (2020).
[17] S. K. Sundaram and E. Mazur, Nat. Mater. **1**, 217 (2002).

[18] K. Matsuda, I. Hirabayashi, K. Kawamoto, T. Nabatame, T. Tokizaki, and A. Nakamura, Phys. Rev. B **50**, 4097 (1994).
[19] V. S. Vikhnin, S. Lysenko, A. Rua, F. Fernandez, and H. Liu, Solid State Commun. **137**, 615 (2006).
[20] B. Torriss, A. Ibrahim, T. Ozaki, and M. Chaker, Phys. Rev. B **98**, 165132 (2018).
[21] S. Iwai, M. Ono, A. Maeda, H. Matsuzaki, H. Kishida, H. Okamoto, and Y. Tokura, Phys. Rev. Lett. **91**, 057401 (2003).
[22] H. Okamoto, H. Matsuzaki, T. Wakabayashi, Y. Takahashi, and T. Hasegawa, Phys. Rev. Lett. **98**, 037401 (2007).
[23] Y. Okimoto, X. Peng, M. Tamura, T. Morita, K. Onda, T. Ishikawa, S. Koshihara, N. Todoroki, T. Kyomen, and M. Itoh, Phys. Rev. Lett. **103**, 027402 (2009).
[24] M. Izquierdo, M. Karolak, D. Prabhakaran, A. T. Boothroyd, A. O. Scherz, A. Lichtenstein, and S. L. Molodtsov, Commun. Phys. **2**, 8 (2019).
[25] M. Rebarz, M. Kloz, S. Espinoza, and C. D. Brooks, UV-VIS-NIR femtosekundový elipsometrický systém, Utility Model No. 30838, Czech Republic, Industrial Property Office (2017).
[26] S. Espinoza, S. Richter, M. Rebarz, O. Herrfurth, R. Schmidt-Grund, J. Andreasson, and S. Zollner, Appl. Phys. Lett. **115**, 052105 (2019).
[27] S. Richter, O. Herrfurth, S. Espinoza, M. Rebarz, M. Kloz, J. A. Leveillee, A. Schleife, S. Zollner, M. Grundmann, J. Andreasson, and R. Schmidt-Grund, New J. Phys. **22**, 083066 (2020).
[28] S. Richter, M. Rebarz, O. Herrfurth, S. Espinoza, R. Schmidt-Grund, and J. Andreasson, Rev. Sci. Instrum. **92**, 033104 (2021).
[29] C. Thomsen, H. T. Grahn, H. J. Maris, and J. Tauc, Phys. Rev. B **34**, 4129 (1986).
[30] D. Fuchs, C. Pinta, T. Schwarz, P. Schweiss, P. Nagel, S. Schuppler, R. Schneider, M. Merz, G. Roth, and H. von Loehneysen, Phys. Rev. B **75**, 144402 (2007).
[31] *Handbook of Ellipsometry*, edited by H. G. Tompkins and E. A. Irene (Andrew, Norwich, NY, 2005).
[32] K. Ishioka, A. Beyer, W. Stolz, K. Volz, H. Petek, U. Hoefer, and C. J. Stanton, J. Phys.: Condens. Matter **31**, 094003 (2019).
[33] M. Dressel, *Electrodynamics of Solids* (Cambridge University Press, Cambridge, 2002).
[34] D. W. Jeong, W. S. Choi, S. Okamoto, J.-Y. Kim, K. W. Kim, S. J. Moon, D.-Y. Cho, H. N. Lee, and T. W. Noh, Sci. Rep. **4**, 06124 (2014).
[35] P. Friš, D. Munzar, O. Caha, and A. Dubroka, Phys. Rev. B **97**, 045137 (2018).
[36] J. Bielecki, A. D. Rata, and L. Borjesson, Phys. Rev. B **89**, 035129 (2014).
[37] C. Thomsen, J. Strait, Z. Vardeny, H. J. Maris, J. Tauc, and J. J. Hauser, Phys. Rev. Lett. **53**, 989 (1984).
[38] K. Asai, O. Yokokura, M. Suzuki, T. Naka, T. Matsumoto, H. Takahashi, N. Mori, and K. Kohn, J. Phys. Soc. Jpn. **66**, 967 (1997).
[39] A. S. Panfilov, G. E. Grechnev, A. A. Lyogenkaya, V. A. Pashchenko, I. P. Zhuravleva, L. O. Vasylechko, V. M. Hreb, V. A. Turchenko, and D. Novoselov, Phys. B (Amsterdam, Neth.) **553**, 80 (2019).
[40] M. Fiebig, K. Miyano, Y. Tomioka, and Y. Tokura, Appl. Phys. B **71**, 211 (2000).
[41] H. T. Grahn, H. J. Maris, and J. Tauc, IEEE J. Quantum Electron. **25**, 2562 (1989).
[42] J. Bielecki, R. Rauer, E. Zanghellini, R. Gunnarsson, K. Dorr, and L. Borjesson, Phys. Rev. B **81**, 064434 (2010).